AEROSOL–CLOUD–METEOROLOGY INTERACTION AIRBORNE FIELD INVESTIGATIONS

Using Lessons Learned from the U.S. West Coast in the Design of ACTIVATE off the U.S. East Coast

Armin Sorooshian, Bruce Anderson, Susanne E. Bauer, Rachel A. Braun, Brian Cairns, Ewan Crosbie, Hossein Dadashazar, Glenn Diskin, Richard Ferrare, Richard C. Flagan, Johnathan Hair, Chris Hostetler, Haflidi H. Jonsson, Mary M. Kleb, Hongyu Liu, Alexander B. MacDonald, Allison McComiskey, Richard Moore, David Painemal, Lynn M. Russell, John H. Seinfeld, Michael Shook, William L. Smith Jr., Kenneth Thornhill, George Tselioudis, Hailong Wang, Xubin Zeng, Bo Zhang, Luke Ziemba, and Paquita Zuidema

Insights and limitations during 500+ flight hours with a single aircraft are used to motivate the dual-aircraft approach in ACTIVATE to study aerosol–cloud–meteorology interactions.

The latest Intergovernmental Panel on Climate Change (IPCC 2013) report stated that the largest uncertainty in estimating global anthropogenic radiative forcing is associated with the interactions of aerosol particles with clouds. Furthermore, the latest Decadal Survey for Earth Science (National Academies of Sciences, Engineering, and Medicine 2017) recommended a designated mission to study aerosols and clouds as one of the "most important" priorities for the Earth observing system. Warm marine boundary layer (MBL) clouds cover more than 45% of the ocean surface (Warren et al. 1998) and consequently exert a large net cooling effect (Hartmann et al. 1992). They are of special interest owing to their pivotal role in unresolved climate change questions associated with climate sensitivity and cloud feedbacks (Mülmenstädt and Feingold 2018). Recent decades have experienced a proliferation of field experiments targeting aerosol–cloud–meteorology interactions for MBL clouds. These labor-intensive, expensive, and challenging efforts have resulted in several datasets that have not been fully exploited because of inconsistencies in measurements and flight strategies between campaigns, and the extensive time and resources needed for quality assurance and in-depth analysis of the vast amount of data collected (Sorooshian et al. 2018). The importance of this research field has been motivated in countless reports and review papers that examine the state of the field and suggest future research needed to help answer some of the most pressing problems (Fan et al. 2016; Seinfeld et al. 2016; Wood et al. 2016; Mülmenstädt and Feingold 2018).

We begin by reflecting on a multiyear effort that aimed to address these limitations by keeping several features in common: i) core group of instruments, ii) a single aircraft, iii) geographic region, iv) time of year, and v) quality control and assurance strategy. The region off the coast of California is one of the most extensively studied for aerosol–cloud–meteorology

interactions owing to proximity to aircraft bases and a wide range in aerosol concentrations coupled to a persistent marine cloud deck, especially in the summertime when experiments are usually conducted. Extensive ship traffic in this study region served as a focal point of many experiments (e.g., Durkee et al. 2000; Russell et al. 2013) since the formation of ship tracks represents one of the clearest visual demonstrations of how aerosol perturbations impact clouds when viewed from space. Diversity of other pollutant sources, with varying characteristic physical and chemical properties, provides an additional benefit for studying this region.

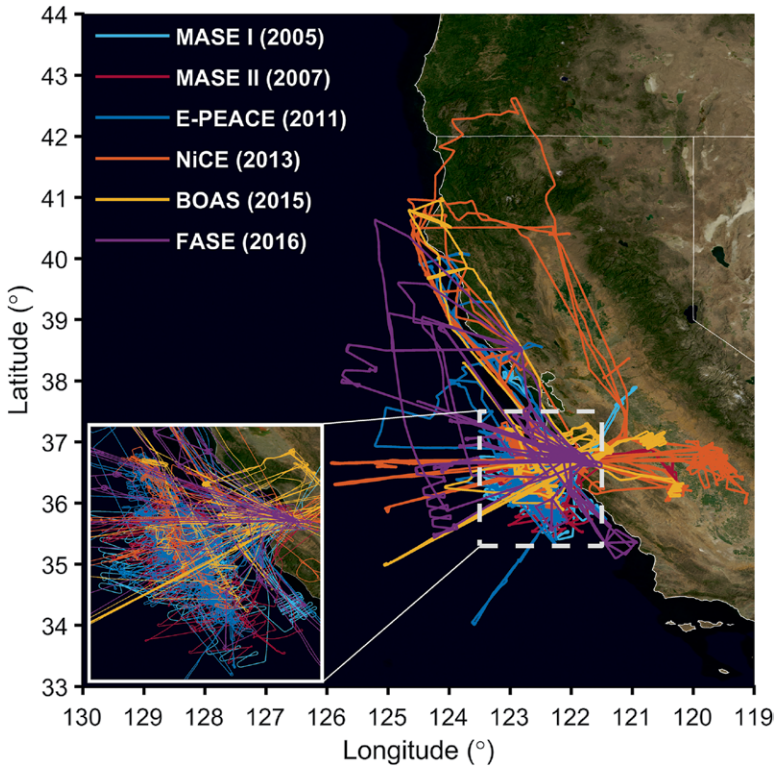

Fig. 1. Summary of flights conducted with the CIRPAS Twin Otter in six summertime campaigns between 2005 and 2016. The coordinates for the expanded white box are 35.3°–37.5°N, 121.5°–123.5°W. (MASE = Marine Stratus/Stratocumulus Experiment; E-PEACE = Eastern Pacific Emitted Aerosol Cloud Experiment; NiCE = Nucleation in Cloud Experiment; BOAS = Biological and Oceanic Atmospheric Study; FASE = Fog and Stratocumulus Evolution Experiment.)

The lessons learned from the California studies sponsored by the Office of Naval Research (ONR) provide motivation for a five-year NASA Earth Venture Suborbital (EVS-3) investigation off the opposite coast of the United States. A dual-aircraft approach with combined in situ and remote sensing instrumentation will be coupled to an unprecedented number of flights to maximize statistics in a region with diverse aerosol and meteorological conditions, including the continuum of warm cloud types spanning stratiform to cumulus. The Aerosol Cloud meTeorology Interactions oVer the western ATlantic Experiment (ACTIVATE) is described in detail, with a description of data analysis and multiscale modeling that will address the complexity of the processes being examined ranging in spatial scale from ~10^{-7} to 10^{6} m (i.e.,

AFFILIATIONS: Sorooshian—Department of Chemical and Environmental Engineering, and Department of Hydrology and Atmospheric Sciences, The University of Arizona, Tucson, Arizona; Anderson, Diskin, Ferrare, Hair, Hostetler, Kleb, Moore, Shook, Smith, and Ziemba—NASA Langley Research Center, Hampton, Virginia; Bauer, Cairns, and Tselioudis—NASA Goddard Institute for Space Studies, New York, New York; Braun, Dadashazar, and MacDonald—Department of Chemical and Environmental Engineering, University of Arizona, Tucson, Arizona; Crosbie, Painemal, and Thornhill—NASA Langley Research Center, and Science Systems and Applications, Inc., Hampton, Virginia; Flagan and Seinfeld—Department of Chemical Engineering, California Institute of Technology, Pasadena, California; Jonsson—Naval Postgraduate School, Monterey, California; Liu and Zhang—National Institute of Aerospace, Hampton, Virginia; McComiske—Brookhaven National Laboratory, Upton, New York; Russell—Scripps Institution of Oceanography, University of California, La Jolla, California; Wang—Atmospheric Sciences and Global Change Division, Pacific Northwest National Laboratory, Richland, Washington; Zeng—Department of Hydrology and Atmospheric Sciences, University of Arizona, Tucson, Arizona; Zuidema—Rosenstiel School of Marine and Atmospheric Science, University of Miami, Miami, Florida
CORRESPONDING AUTHOR: Armin Sorooshian, armin@email.arizona.edu

The abstract for this article can be found in this issue, following the table of contents.
DOI:10.1175/BAMS-D-18-0100.1

A supplement to this article is available online (10.1175/BAMS-D-18-0100.2)

In final form 1 April 2019

single particle to synoptic scale). We conclude with a preview of how the generated results can be used by the research community.

COASTAL CALIFORNIA FLIGHTS. Data were collected using the Center for Interdisciplinary Remotely-Piloted Aircraft Studies (CIRPAS) Twin Otter on 113 flight days for a total of 514 flight hours in the areas shown in Fig. 1. The payload is summarized in Table ES1 (https://doi.org/10.1175/BAMS-D-18-0100.2) with datasets provided by Sorooshian et al. (2017, 2018). The general flight pattern included level legs at various altitudes (below cloud, in cloud at different levels, above cloud) with occasional vertical soundings as either slants or spirals (Fig. 2). The level legs (~10–15 min) were meant to generate statistics at a fixed altitude, in addition to providing sufficient time for measurements with longer time resolutions (e.g., cloud water collection, scanning mobility particle sizers) and enhancing accuracy of measurements requiring the aircraft to remain level (e.g., wind measurements). The soundings (~10–15 min at an incline rate of 90 m min^{-1}) were useful for characterizing the vertical environmental profile. For the full set of calculations desired for aerosol–cloud interactions in these campaigns, it was necessary to have data below, in, and above clouds, which amounted to a total of 297 cases, hereinafter referred to as "cloud events." This number was reduced from the 439 events sampled owing to lack of data or poor data quality for at least one of the requisite parameters.

Histograms of relevant parameters for aerosol–cloud interactions demonstrate the wide range of conditions that have drawn researchers to study the coastal California region (Fig. 3). The boundary layer height for the coastal California clouds can be extremely shallow (Zuidema et al. 2009), with cloud-top heights (CTHs) ranging in these flights between 135 and 1,150 m, with a mean of 541 m. Cloud depths and liquid water paths (LWPs) ranged between 40 and 760 m and 10 and 310 g m^{-2}, respectively. Clouds were typically subadiabatic (average adiabaticity = 0.766 ± 0.134; Braun et al. 2018). On average, the observed LWC lapse rate tended to be a fairly constant fraction of the adiabatic LWC lapse rate through the bottom 90% by height of the cloud; however, in the top 10% of the cloud, a sharp decrease in LWC was observed [Fig. 4 of Braun et al. (2018)], most likely due to processes such as cloud-top entrainment and precipitation. Cloud droplet number concentrations N_d reached as low as ~20 cm^{-3} and as high as ~400 cm^{-3}. This broad range is driven by variability in out-of-cloud aerosol levels, with both sub- and above-cloud Passive Cavity Aerosol Spectrometer Probe (PCASP) concentrations D_p (~0.1–2.6 μm) spanning three orders of magnitude. Aside from sea spray and marine biogenic sources of aerosols (Modini et al. 2015), ship exhaust was a major subcloud source (Coggon et al. 2012; Wang et al. 2014). The major sources impacting the above-cloud aerosol budget were transported continental emissions of wildfire plumes (Maudlin et al. 2015; Mardi et al. 2018), dust, biogenic secondary organic aerosol (SOA), and urban pollution (Hegg et al. 2010; Prabhakar et al. 2014; Wang et al. 2014). The aerosols above cloud in the

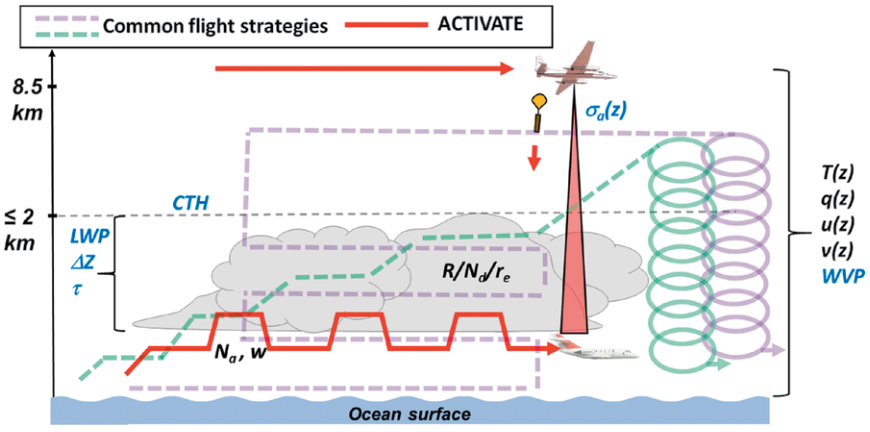

Fig. 2. Flight strategies employed by a single Twin Otter aircraft in previous aerosol–cloud field investigations (dashed green and purple lines), in contrast to the comprehensive plan for ACTIVATE using a dual-aircraft approach (red lines). Relevant parameters that are typically needed for analysis are shown where they are measured, with some values integrated over cloud depth and others as a function of altitude [i.e., *f*(z)]: LWP = liquid water path, WVP = water vapor path, ΔZ = cloud thickness, τ = cloud optical depth, CTH = cloud-top height, N_a = subcloud aerosol concentration, *w* = cloud base updraft velocity, *R* = rain rate, N_d = cloud droplet concentration, r_e = drop effective radius, σ_a = vertically resolved remote sensing parameters such as aerosol extinction coefficient, *T* = temperature, *q* = humidity, *u*/*v* = wind components. Variables in blue and black are measured via remote sensing and in situ techniques, respectively; note though that *T*(z), *q*(z), *u*(z), and *v*(z) are measured with dropsondes released from the higher aircraft.

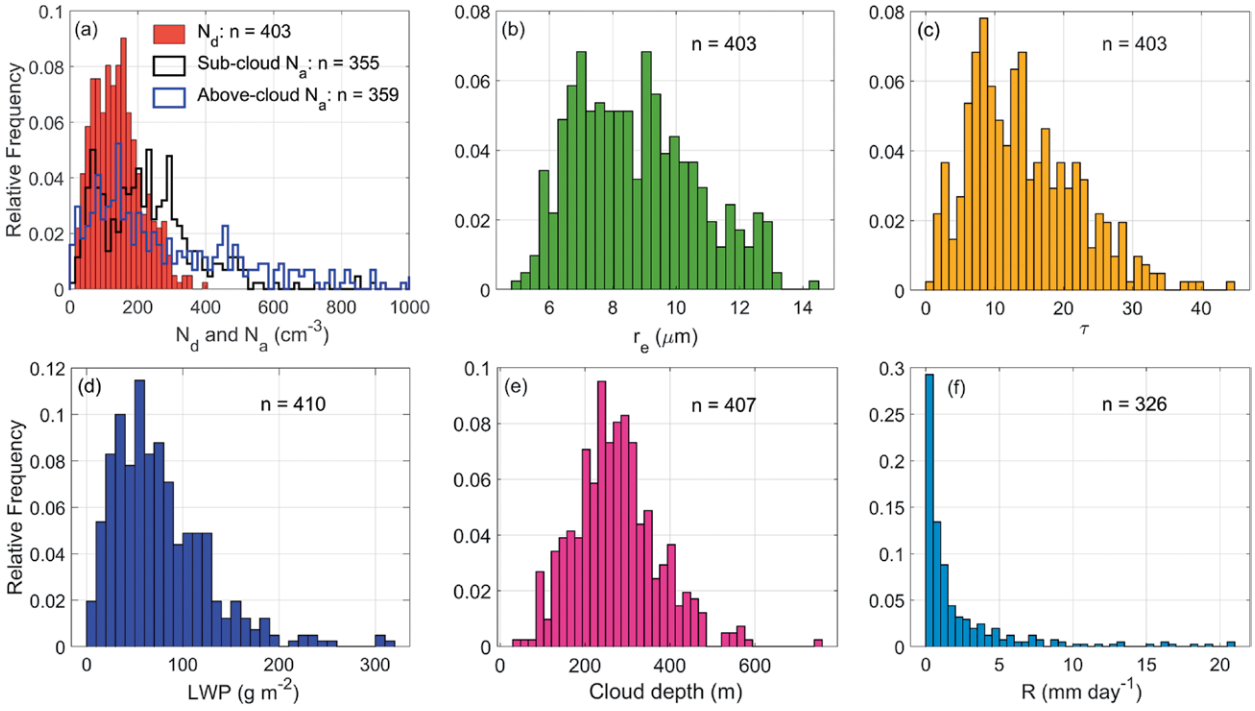

Fig. 3. Histograms summarizing the range of conditions associated with aerosol and cloud parameters during the six Twin Otter campaigns. Some of the *x* axes extend to higher values but are truncated here to better represent the variability of the majority of the cases. Values for N_d, r_e, τ, LWP, cloud depth, and *R* represent cloud-columnar mean values.

free troposphere had a distinctly different chemical signature than below cloud owing to greater organic mass fractions and thus less hygroscopic aerosol (Hersey et al. 2009). The very thin (tens of meters) entrainment interface layer (EIL) immediately above cloud top and below the free troposphere contained a mixture of free tropospheric particles, boundary layer particles processed by clouds, and nucleated particles (Dadashazar et al. 2018).

In situ measurements in these campaigns provided insights into a number of key processes illustrated in Fig. 4 through the use of case study flights that probed specific questions related to the ways in which aerosols impact clouds and clouds impact aerosols, the underlying effect of meteorology on both types of interactions, and the intrinsic coupling between aerosols and cloud droplets that affects the formation and loss of both. A series of three flights helped to unravel some of the details associated with large stratocumulus cloud clearings, which exhibit intriguing diurnal characteristics such as growth in clearing area during the day and contraction at night (Crosbie et al. 2016). Another series of flights explored why ship tracks are not observable from space on all single-layer cloud days, including the influence of mesoscale cloud structure and free tropospheric humidity (Chen et al. 2012). Strategic flight patterns immediately behind cargo and tanker ships revealed significant amounts of giant cloud condensation nuclei (CCN; giant CCN is defined here as having diameters >2 μm) emitted via some combination of wave breaking and stack exhaust (Sorooshian et al. 2015a); even low levels of giant CCN can reduce cloud albedo via enhanced collision–coalescence, offsetting the impact of the smaller CCN in ship exhaust (Feingold et al. 1999; Jung et al. 2015). As wind directions became favorable for blowing continental emissions (e.g., dust, urban pollution, wildfire plumes) over the stratocumulus deck, opportunities arose to identify chemical pathways of organo-nitrogen (Sorooshian et al. 2009a; Youn et al. 2015), organo-sulfur (Sorooshian et al. 2015b), and organic acid (Sorooshian et al. 2007, 2010a) production in addition to already documented sources from marine biogenic emissions. Free-tropospheric aerosols and fresh smoke with high organic mass fractions were coincident with suppressed aerosol hygroscopicity at relative humidity >70% (Hersey et al. 2009; Wonaschütz et al. 2013) and sometimes revealed reductions in particle size after humidification owing possibly to particle restructuring and/or volatilization effects (Shingler et al. 2016). The various case studies of aerosol impacts on clouds have been

assisted in great part by chemical measurements of both cloud water, such as with the Axial Cyclone Cloud Water Collector (AC3; Crosbie et al. 2018), and droplet residual particles (e.g., Sanchez et al. 2016) with a Counterflow Virtual Impactor inlet (Shingler et al. 2012). These measurements have also been instrumental in advancing knowledge of cloud impacts on aerosol including wet scavenging (MacDonald et al. 2018) and chemical, collisional, and coalescence processing (Sorooshian et al. 2007, 2013; Ervens et al. 2014; Asa-Awuku et al. 2015; Weiss-Penzias et al. 2018).

Aside from case studies, important analyses can be conducted using the full set of data and statistics such as for constraining the values of aerosol–cloud interaction (ACI) metrics that relate to model parameterizations. Changes in cloud droplet number concentration N_d with an aerosol number concentration proxy α [ACI_N in Eq. (1)] can be related to droplet activation, where ACI_N values range from 0 to 1, with higher values signifying activation of relatively more aerosol particles into cloud droplets. A parameter used in place of the aerosol proxy α is often the subcloud aerosol concentration N_a, which is derived from the PCASP in this analysis. The relationship between the cloud microphysical state (cloud droplet effective radius r_e) and the subcloud aerosol environment can additionally be quantified with Eq. (2) (ACI_{r_e}), which is theoretically bounded by 0 and 0.33 ACI_{r_e} as = 1/3 ACI_N at fixed LWP (Feingold et al. 2001). Variations in precipitation rate R as a function of N_d [precipitation susceptibility S_o in Eq. (3)] provide a metric for evaluating autoconversion in models, where higher values of S_o indicate that for a fixed increase in N_d, R is more strongly suppressed. A large and robust statistical dataset provides more opportunities for holding nonaerosol factors fixed, which is required to isolate the impact of aerosol perturbations on cloud properties. Studies that focus on a specific cloud regime implicitly reduce the effect of meteorology (e.g., sea surface temperature (SST), lower troposphere stability (LTS), horizontal advection, large-scale subsidence) on the ACI calculation. In addition, control for the cloud dynamics can to some extent be achieved by binning the observations as a function of cloud thickness (e.g., Lu et al. 2009) or LWP (e.g., Lu et al. 2009; Painemal and Zuidema 2013), as in Eqs. (2) and (3) ($|_{LWP}$):

$$ACI_N = \frac{d\ln(N_d)}{d\ln(\alpha)}, \quad (1)$$

$$ACI_{r_e} = -\left.\frac{\partial\ln(r_e)}{\partial\ln(\alpha)}\right|_{LWP}, \quad (2)$$

$$S_o = -\left.\frac{\partial\ln(R)}{\partial\ln(N_d)}\right|_{LWP}. \quad (3)$$

Figure 5a shows that ACI_N is 0.51 ± 0.06, which is similar to the average value obtained by surface-based measurements in the same coastal region (0.48), but in contrast with values reported for stratiform clouds in several other regions (0.63–0.99) (McComiskey et al. 2009, and references therein). Higher values of ACI_N indicate that N_d is more enhanced for a fixed increase in N_a, with reasons for differences including choice of proxy for α, relative range of LWP and N_a observed, scale of analysis, cloud base updraft velocity, and aerosol size distribution and composition (McComiskey et al. 2009). Mean values of ACI_{r_e} varied considerably from as low as 0.04 to as high as 0.25 with significant standard deviations in the last three LWP bins (140–160, 160–180, 180–320 g m^{-2}) due to reduced sample sizes. Reduced ACI_{r_e} values at the highest LWP values can be linked at least partly to increased collision–coalescence, drizzle,

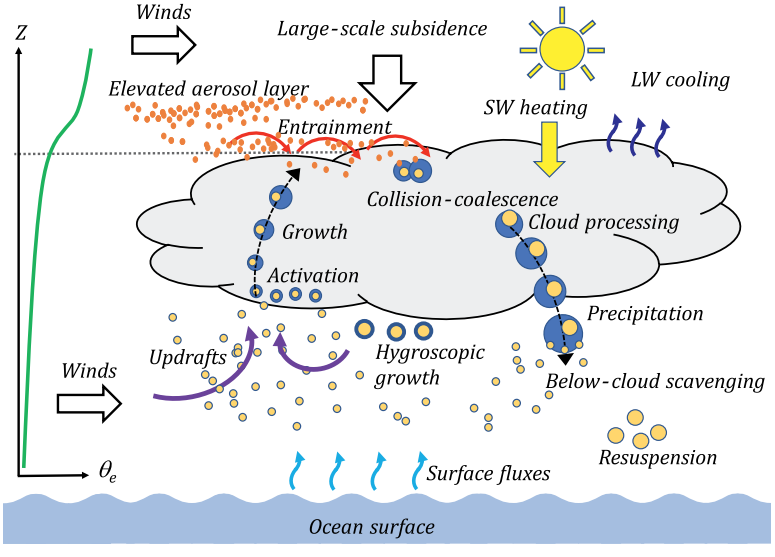

Fig. 4. Airborne field campaigns, including especially those with the Twin Otter and the upcoming ACTIVATE mission, aim to improve understanding and model representations of these illustrated aerosol–cloud–meteorology interactions; Z and q_e represent altitude and equivalent potential temperature, respectively.

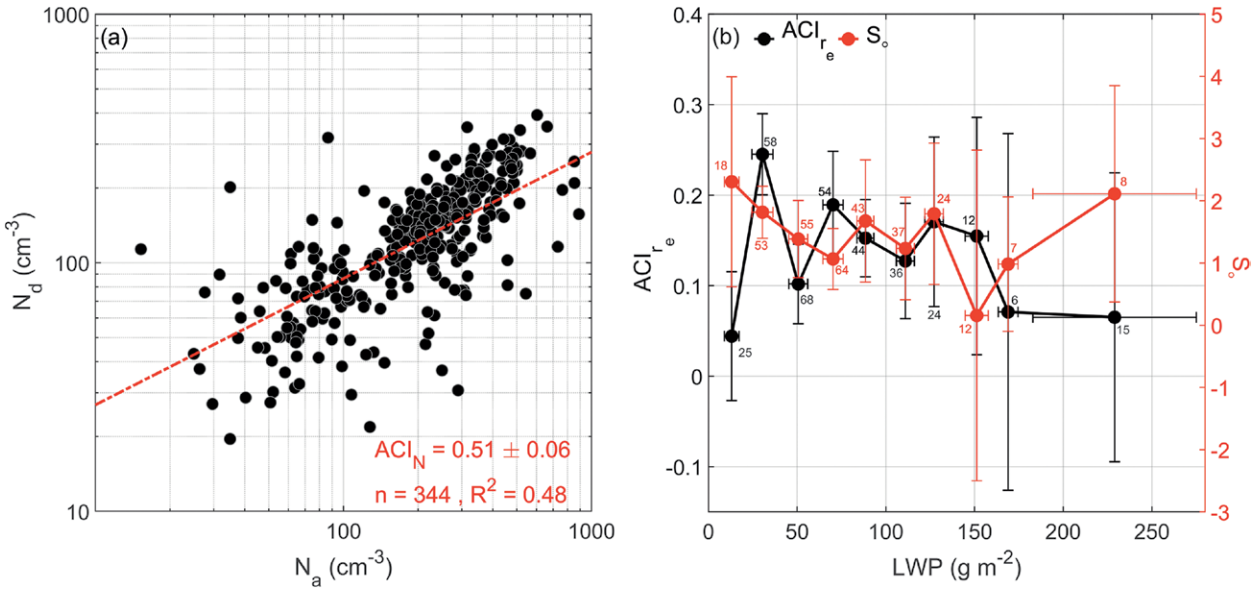

Fig. 5. Aerosol–cloud interactive analyses using the cumulative dataset from the Twin Otter campaigns. (a) Comparison of N_d vs N_a, where the slope is equal to ACI$_N$ in Eq. (1). (b) LWP-dependent values of aerosol–cloud interaction metrics defined in Eqs. (2) and (3). The number of data points used for quantification of S_o and ACI$_{r_e}$ in each LWP bin is shown in red and black, respectively. A major limitation in the campaigns was the lack of statistics to bin the data in tighter LWP bins and to hold other nonaerosol factors fixed to reduce the size of the standard deviations.

and scavenging (McComiskey et al. 2009). Values of S_o ranged from 0.16 to 2.31 with a mean of 1.45 ± 0.63. The LWP-dependent trend and absolute values of S_o cannot be intercompared in an "apples to apples" sense to other studies (e.g., Sorooshian et al. 2009b, 2010b; Bangert et al. 2011; Terai et al. 2012, 2015; Gettelman et al. 2013; Mann et al. 2014) due to the sensitivity of the results to factors highlighted in a number of studies (Duong et al. 2011; Feingold et al. 2013; Lebo and Feingold 2014) and variability owing to whether results came from aircraft, remote sensing, or modeling. Noteworthy though is that others have provided observational and theoretical justification for S_o decreasing with LWP for stratocumulus clouds (e.g., Wood et al. 2009; Terai et al. 2015). The fact that numerous works now show that S_o varies with LWP and cloud thickness raises alarm for the use of a simple power law treating autoconversion in models ($R \sim \text{LWP}^{\alpha} N_d^{-\beta}$), which assumes S_o (equivalent to β at fixed LWP) is fixed with a value often set to 1.79 (Khairoutdinov and Kogan 2000).

A number of factors need to be considered with regard to the i) applicability of these results to models, ii) intercomparison with other studies relying on different approaches and datasets, in particular from remote sensing, and iii) identification of the source of the large standard deviations in Fig. 5. These factors include the i) impact of wet scavenging and above-cloud aerosol layers on the independent variable of Eqs. (1)–(3) (Duong et al. 2011; Coggon et al. 2014; Prabhakar et al. 2014; Dadashazar et al. 2018; MacDonald et al. 2018); ii) choice of how to calculate parameters such as LWP, α, N_d, r_e, and R (e.g., Lu et al. 2009; Jung et al. 2016); iii) degree of cloud coupling to the surface layer (Crosbie et al. 2016; Wang et al. 2016); iv) cloud contact time (Feingold et al. 2013); v) cloud lifetime (Jiang et al. 2010); vi) absolute value of the N_a range examined (Feingold et al. 2013); vii) presence of giant CCN (Dadashazar et al. 2017); viii) turbulence (Terai et al. 2015); and ix) scale (McComiskey and Feingold 2012; Mülmenstädt and Feingold 2018). Other factors likely exist that coincide with in-cloud adjustments that absorb or "buffer" the system to aerosol perturbations (Stevens and Feingold 2009). More statistics across a range of values for parameters such as N_a, LWP, and LTS are necessary to better constrain the values of such metrics for cloud types other than stratiform, which have been the focus of major field efforts off the western coasts of North America, South America (Mechoso et al. 2014), and southern Africa.

The Twin Otter campaigns have been very successful in advancing knowledge of aerosol–cloud–meteorology interactions for stratocumulus clouds off the California coast, but a number of challenges motivate the need for a new approach in order to

improve our understanding of such interactions across all warm cloud regimes. While the wide aerosol variability in coastal California has been advantageous for certain studies, one limitation has been the narrow conditions of high LTS and low LWP (Fig. 3) observed in the region. A single aircraft also has limited ability to simultaneously acquire all the necessary data in a column (below, in, and above cloud). For instance, more flight time is typically allocated to level legs used to characterize aerosol and cloud properties, leaving fewer opportunities for vertical soundings needed for in situ data to calculate LWP (Fig. 2). Also, even with 514 flight hours, sample sizes were still sufficiently small to lead to large standard deviations for metrics in Fig. 5 for each LWP bin; with more statistics, LWP bins could be made narrower and additional parameters [e.g., LTS, SST, horizontal advection, large-scale subsidence] could also be held fixed to better isolate the aerosol influence on clouds. The use of multiple aircraft allows for simultaneous in situ and remote sensing data collection, with the significant caveat that the aircraft must not have significantly different air speeds.

ACTIVATE: A NEW PATH FORWARD. ACTIVATE is motivated by the limitations noted above associated with statistics, measurement obstacles, and regional characteristics. Furthermore, ACTIVATE follows the Decadal Survey's recommendation to target specific cloud types and integrate multiplatform observations with modeling activities (National Academies of Sciences, Engineering, and Medicine 2017); in particular, the combined deployment of a lidar and polarimeter on an airborne platform is considered a top priority for advancing aerosol–cloud science (National Academies of Sciences, Engineering, and Medicine 2017). A key component of ACTIVATE is the planned 150 joint flights between two closely coordinated aircraft with similar airspeeds for acquiring simultaneous, collocated in situ and remote sensing measurements that reduce sampling differences; this will amount to ~600 joint total flight hours for each aircraft conducted over three years. An advancement that will be leveraged by ACTIVATE is the enhanced maturity of remote sensing retrievals of aerosol and cloud properties, which fill a primary measurement role that complements, rather than duplicates, in situ measurements. More specifically, past EVS missions [i.e., Deriving Information on Surface Conditions from Column and Vertically Resolved Observations Relevant to Air Quality (DISCOVER-AQ) and North Atlantic Aerosols and Marine Ecosystems Study (NAAMES)] helped with the development and validation of such retrievals versus contemporaneous and collocated in situ measurements (e.g., Sawamura et al. 2017; Alexandrov et al. 2018). Planned flights will take place between February–March and May–June between 2020 and 2022. ACTIVATE's three main objectives are as follows:

- Objective 1. Quantify relationships between N_a, CCN concentration, and N_d, and reduce uncertainty in model parameterizations of cloud droplet activation.
- Objective 2. Improve process-level understanding and model representation of factors that govern cloud micro-macrophysical properties and how they couple with cloud effects on aerosol.
- Objective 3. Assess advanced remote sensing capabilities for retrieving aerosol and cloud properties related to aerosol–cloud interactions.

Why the western North Atlantic? The choice of region is important for a multiyear campaign that aims to generate significant statistics targeting a wide range in aerosol variability of natural and anthropogenic sources, and meteorological conditions, in addition to the presence of different cloud types. The western North Atlantic Ocean region is subject to a distinct and undersampled range of LTS. This gives rise to wider LWP variability as compared to subtropical stratiform marine regions (Fig. 6). Shallow cumulus clouds constitute the major low-cloud weather state (e.g., Tselioudis et al. 2013) with a frequency of occurrence of about 17%. Marine stratocumulus cloud regimes are less frequent in the region, occurring on average around 6% of the time, in contrast with the eastern ocean boundary regions where their frequency of occurrence is near 36%. The ability to study MBL clouds spanning the continuum of stratiform to cumulus clouds includes focused sampling of cloud types with particularly strong modeling challenges, namely, postfrontal clouds and associated cold air outbreaks (Field et al. 2014, 2017).

The ACTIVATE domain (25°–50°N, 60°–85°W) is one of the oceanic regions that has undergone the largest increase in aerosol burden and N_d since preindustrial times (Merikanto et al. 2010; Bauer and Menon 2012; Lee et al. 2016). Although there has been a decrease in the aerosol burden since the early 1980s (Yoon et al. 2014), the ACTIVATE domain is still significantly impacted by aerosol transport from the continental United States (Stamnes et al. 2018). The region is characterized by the importance of aerosol effects on cloud feedbacks on climate (Gettelman and

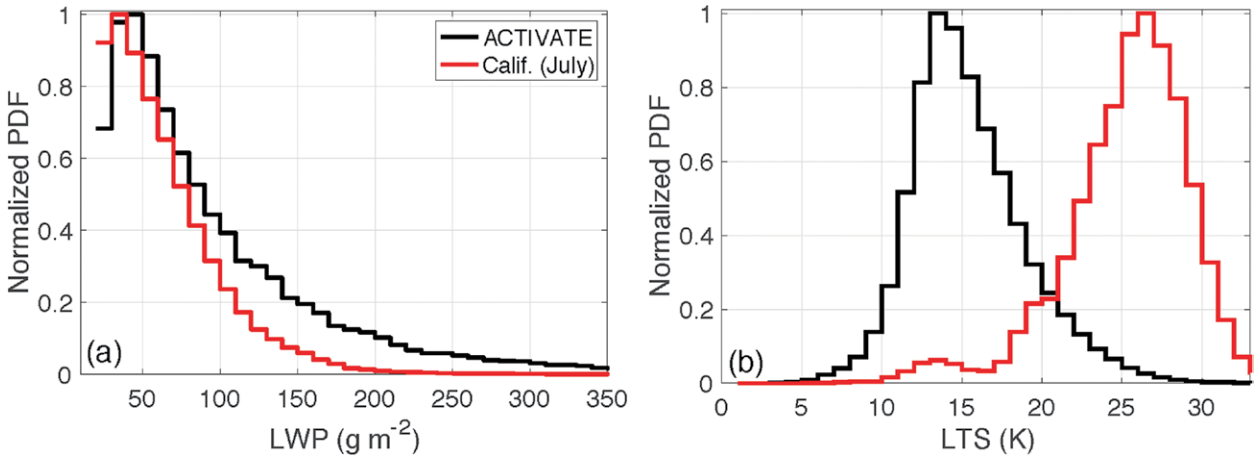

Fig. 6. Normalized probability density function (PDF) of (a) daily 1° × 1° MODIS LWP and (b) daily 0.625° × 0.5° MERRA-2 LTS for the northeast Pacific (30°–37°N, 110°–130°W; red) during Jul, and an oceanic subdomain (30°–45°N, 65°–78°W; black) of the ACTIVATE region during the combined Feb–Mar and May–Jun periods (2010–15). The ACTIVATE data reveal a greater LWP range and a distinct and undersampled LTS regime ideal for developing more robust parameterizations.

Sherwood 2016). ACTIVATE will evaluate CCN and N_d parameterizations across the full dynamic range of continental to clean marine conditions (Figs. 7c–f), with zonal gradients evident based on aerosol optical depth (AOD) and N_d for the different 2-month flight periods planned (February–March, May–June; e.g., Figs. 7a,b and 8a). Diverse emission sources include anthropogenic and biogenic emissions from the Eastern Seaboard, sea salt and marine biogenic emissions, shipping, and even Saharan dust (Castanho et al. 2005) that collectively give rise to an aerosol gradient between the coast and mid-Atlantic. The North Atlantic also experiences ultraclean conditions (<20 cm^{-3}) associated with North Atlantic postfrontal clouds (Wood et al. 2017). This wide range of CCN concentrations, from pristine to polluted conditions, provides a range of cloud susceptibilities to increases in CCN (Koren et al. 2014), which, while it may not replicate the preindustrial state, provides a valuable dataset for evaluating whether model simulations of that state are plausible (Hamilton et al. 2014). This is important because estimates of effective radiative forcing associated with aerosol–cloud interactions are based on comparing present day forcing to preindustrial times. To obtain data representative of the latter, field campaigns have focused on clean remote areas such as the Southern Ocean (McCoy et al. 2015; Seinfeld et al. 2016). The ACTIVATE region can mimic such conditions in a more readily accessible location.

Changes in cloud albedo attributed to fractional increases in N_d (Fig. 8b) peak near the coast, suggesting a link between N_d and albedo enhancement, mediated by changes in aerosol loading. While aerosol–cloud interaction signatures are apparent over the ACTIVATE domain, this region departs from other MBL regimes in some significant ways. For instance, the mean satellite-derived LWP (Fig. 6) and CTH (Fig. 8d) feature greater spatial variability (30–120 g m^{-2} and 1,400–2,400 m, respectively) than that typically observed in eastern oceanic stratocumulus cloud regimes in the subtropics (Bennartz 2007; Zuidema et al. 2009). This advantageously extends the range of available conditions, which is a critical component of understanding how aerosol susceptibility metrics covary with meteorological regime. In addition, cloud fraction less than 60% (Fig. 8c) often occurs in the ACTIVATE region, and is favorable for the near-collocated remote sensing of both clouds and vertical aerosol structure.

A critical feature of the wintertime meteorology affecting the western North Atlantic Ocean is the frequent passage of cold fronts, which can induce prominent low-level cold-air advection (cold air outbreaks) across the coastal waters. During these events, strong surface heat and moisture fluxes establish predictable and widespread offshore gradients in the MBL, including cloud structure and associated thermodynamic properties, making these events favorable targets for repetitive sampling. Although less temporally persistent, winter/spring season cold air outbreaks could be considered as a canonical cloud regime in the ACTIVATE sampling domain similar to how the summertime stratocumulus deck is for eastern subtropical oceans. Postfrontal clouds are underrepresented in climate model simulations over

the North Atlantic region, with models showing shallow cumulus (mostly postfrontal) cloud coverage at only a few percent compared to remote sensing observations of 15%–20% (Remillard and Tselioudis 2015). Furthermore, numerical challenges also extend to weather forecast models, with Field et al. (2014) showing poor model prediction of shallow stratiform clouds and an overall underestimation of LWP during a specific North Atlantic cold air outbreak. The underprediction of coverage of shallow cumulus clouds in the cold-air sector is a generic problem with climate model representations of postfrontal clouds in both the Northern and the Southern Hemispheres (Williams et al. 2013; Bodas-Salcedo et al. 2014). We therefore expect the results from ACTIVATE, insofar as they can be used to improve the simulation of shallow cumulus clouds in the cold-air sector, to also be relevant to the Southern Ocean. Improving the simulation of these clouds is a particular focus of ACTIVATE, because the primary reason for the excess of solar radiation reaching the Southern Ocean surface predicted in most models (Trenberth and Fasullo 2010) is the low cloud cover in the cold-air

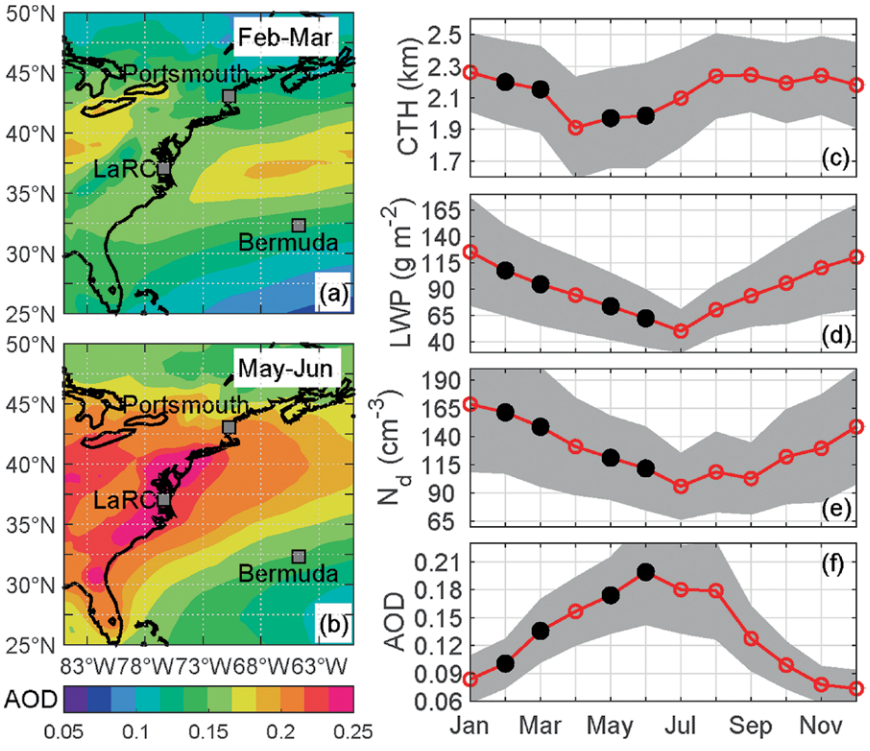

Fig. 7. MERRA-2 (2003–17; Randles et al. 2017) climatology of AOD over the western North Atlantic Ocean for the two 2-month periods that ACTIVATE will target: (a) Feb–Mar and (b) May–Jun. Mean annual time series (2003–17) are shown for *Aqua* MODIS-derived parameters including (c) CTH, (d) cloud LWP, (e) N_d, and (f) AOD. CERES Edition 4 was used for cloud retrievals (Minnis et al. 2011) and Collection 6 was used for AOD (Levy et al. 2013). In addition, the AOD time series only includes data with cloud fraction less than 0.5 (50%), whereas the cloud property time series are for overcast pixels. Gray areas correspond to the monthly standard deviation. The ACTIVATE periods are denoted by black markers, which capture the wide range in AOD, N_d, and cloud properties desired for building robust model parameterizations.

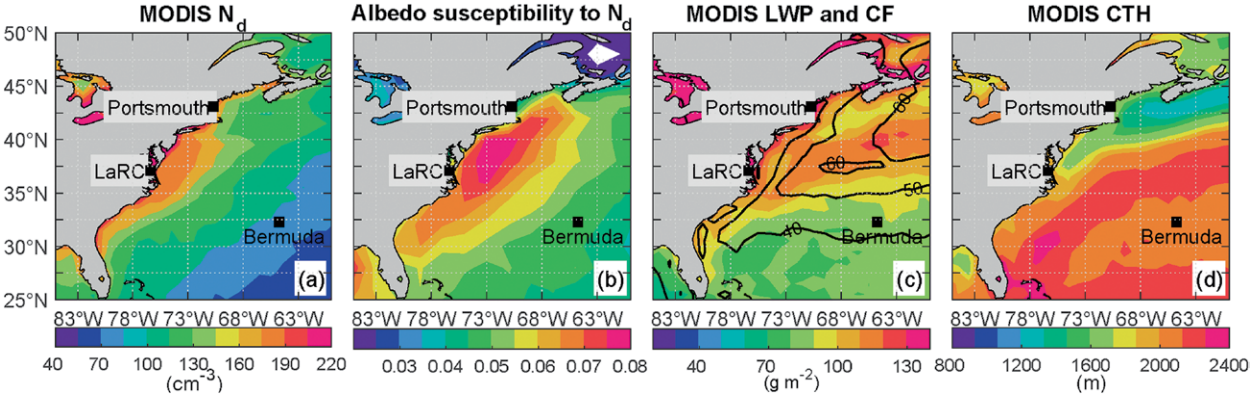

Fig. 8. Satellite-based annual-mean climatology of low-cloud properties over the western North Atlantic Ocean region for (a) MODIS N_d, (b) CERES cloud albedo susceptibility to fractional changes in N_d (Painemal 2018), (c) MODIS LWP (in colors) and cloud fraction (contours), and (d) MODIS CTH.

sector and this excess of radiation leads to erroneous simulation of temperature and affects the accuracy of modeling current and future climate.

A more comprehensive approach. To address the issue of statistics, ACTIVATE will deploy two complementary NASA Langley Research Center (LaRC) aircraft flown simultaneously over the same region but at two different altitudes: a low-flying HU-25 Falcon (minimum altitude of 0.15 km) and higher-flying B-200 King Air (nominal flight altitude of 9 km; see sidebar "Flight types"). The payload summaries for both aircraft are provided in Table ES1 to contrast with that from the Twin Otter campaigns. The HU-25 payload focuses on acquiring detailed in situ aerosol, cloud, precipitation, and meteorological state parameters below, within, and above MBL clouds. The B-200 will simultaneously acquire remote sensing retrievals of aerosols and clouds and deploy dropsondes to measure the vertical profile of the meteorological state parameters. ACTIVATE's two-aircraft approach can capture all necessary data for the equivalent of a Twin

FLIGHT TYPES

Two flight profiles will be employed during ACTIVATE to maximize sampling of low cloud regimes that are known sources of model uncertainty in low cloud simulations. Weather state analysis will be performed in the flight planning stages (e.g., Tselioudis et al. 2013; Remillard and Tselioudis 2015) to identify the cloud regimes that will be expected to be sampled by the planned flight patterns. The "statistical survey" pattern (Fig. SB1a) involves close coordination between both aircraft to provide near coincident sampling of N_d, CCN concentration, and/or N_a at and below cloud base and above and within cloud top. This dual-aircraft pattern provides more than twice the amount of data that could be obtained using only a single aircraft, which must reverse course and fly at both low and high altitudes to allow in situ and remote sensors to sample the same region. The nominal statistical survey vertical profiles are shown in Fig. SB1c.

Approximately 10% of the ACTIVATE flights (~60 joint flight hours) will target intensive sampling in localized (~100 km × 100 km) regions focused on specific cloud systems (e.g., postfrontal clouds); the presence of those systems and desirable weather will be used in decisions of when to do "process study" flights. The process study flight pattern (Fig. SB1b) used for these flights includes vertical profiles of the HU-25 ranging from 0.15 to ~3 km as shown in Fig. SB1d. The dots in Fig. SB1b represent dropsonde locations (10–15 dropsondes throughout the sampling region) deployed from the B-200. This pattern is optimized for large-eddy simulation studies. Flight patterns will also be executed to acquire data under satellite sensors (e.g., CALIOP, ATLID, VIIRS) as satellite tracks and conditions warrant.

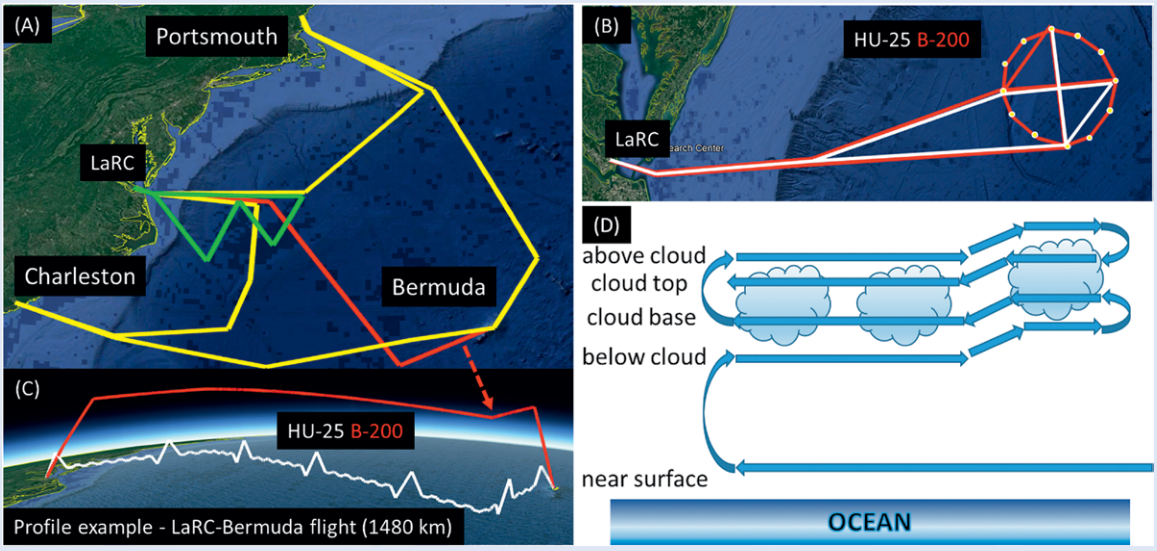

Fig. SB1. Example of the (a),(c) statistical survey and (b),(d) process study flight patterns from the primary base (LaRC) and secondary bases (Charleston, Portsmouth, and Bermuda) of operations, with (d) being specifically for the low-flying aircraft. The colors in (a) distinguish the different patterns: yellow shows flights between potential secondary bases, red is the same and is highlighted to match the profile shown in (c), and green is a local flight from LaRC (similar local flights from secondary bases are possible but not shown). These flight patterns show the flexibility and range for intensive MBL cloud sampling to address ACTIVATE objectives.

Otter cloud event (~90 min) in ~10 min, which includes a few minutes both below and in cloud with the low-flying aircraft and a steady altitude with the high-flying aircraft (Fig. 9).

A particular strength of the B-200 payload will be the simultaneous deployment of the High Spectral Resolution Lidar-2 (HSRL-2) and the Research Scanning Polarimeter (RSP). These instruments have flown together on this aircraft over the western North Atlantic Ocean during the Department of Energy (DOE) Two-Column Aerosol Project (TCAP; Berg et al. 2016) and over the southeastern Atlantic Ocean during the NASA ORACLES deployments (e.g., Xu et al. 2018). HSRL-2 data acquired during TCAP were used to i) characterize the vertical distribution of aerosols and AOD in this region (Berg et al. 2016); ii) evaluate the ability of WRF-Chem v3.7 and CAM5 v5.3 models to simulate profiles of aerosol properties (Fast et al. 2016); iii) demonstrate the ability of multiwavelength lidar measurements to retrieve profiles of aerosol effective radius and aerosol number, surface, and volume concentrations (Müller et al. 2014); and iv) validate AOD retrievals derived from the RSP measurements (Stamnes et al. 2018). Modifications to HSRL-2 performed prior to ACTIVATE will enable the acquisition of very high vertical resolution (1.25 m) data, similar to HSRL-1 during the Ship-Aircraft Bio-Optical Research (SABOR) and NAAMES missions (Hostetler et al. 2018). This capability also enables retrievals of cloud-top extinction profiles and cloud-top lidar ratios (ratio of extinction to backscatter) as well as profiles of particulate backscatter, extinction, and depolarization below the ocean surface (Hair et al. 2016; Schulien et al. 2017). RSP data have been used to derive aerosol properties such as AOD, effective radius, single-scattering albedo, and refractive index (Stamnes et al. 2018; Xu et al. 2018), as well as cloud drop size distributions together with parametric retrievals of effective radius and variance (Alexandrov et al. 2012, 2018). The RSP capability to retrieve cloud optical depth τ simultaneously with remote sensing and in situ cloud microphysical properties provides the connection between aerosol–cloud physical processes and their radiative manifestations needed to clarify the impact on atmospheric energy balances.

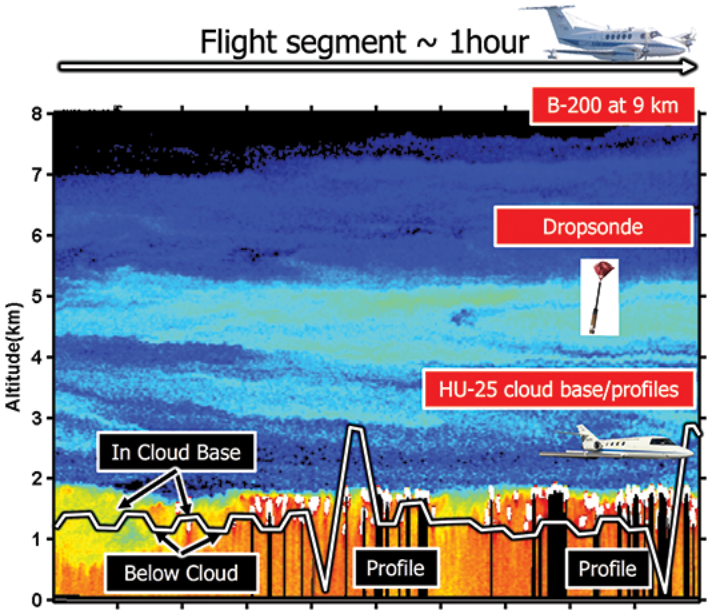

Fig. 9. A representative hour of an ACTIVATE flight to efficiently capture data needed for calculations of aerosol–cloud–meteorology interactions. The B-200 and HU-25 flight altitudes are overlaid on an image showing aerosol and cloud backscatter measured by HSRL-1 (an earlier generation of HSRL-2) over the southwest Atlantic Ocean on 23 May 2007 during a CALIOP validation flight. The B-200 has a constant nominal flight altitude of 9 km while the HU-25 conducts boundary layer and cloud sampling between 0.15 and 3 km. Coordination of both aircraft are within ~1–2 km (between aircraft tracks) and 10 min. The nominal ground speed of both aircraft flying at their respective altitudes planned for the ACTIVATE patterns is 120 m s^{-1}.

The combination of HSRL-2 retrievals of cloud-top extinction and RSP retrievals of cloud-top droplet size distribution enables an additional and unique retrieval of cloud-top N_d and LWC without assumptions about cloud adiabaticity. The recent NAAMES campaigns, noted above, provided an opportunity to evaluate these cloud-top size retrievals (Alexandrov et al. 2018) and also allowed initial comparisons of the cloud-top extinction from the lidar. Comparisons were made to in situ cloud droplet size distributions and N_d measured by a cloud droplet probe (CDP) that sampled within the same cloud during stacked aircraft flight profiles. The vertical profiles of aerosols from the lidar, detailed cloud-top size distributions from the polarimeter, and combined instrument retrievals of LWC and N_d on a single aircraft during ACTIVATE enable a unique opportunity to diagnose cloud-top (typically top 50–100 m) autoconversion rates (e.g., Wood 2005) and mixing processes at cloud top (Liu and Daum 2004). Moreover, by deploying the HSRL-2 instrument,

which measures profiles of backscatter at 355, 532, and 1,064 nm and extinction via the HSRL technique at 355 and 532 nm, ACTIVATE bridges the existing Cloud–Aerosol Lidar with Orthogonal Polarization (CALIOP; 532, 1,064 nm) to planned [Earth Clouds, Aerosols and Radiation Explorer–Atmospheric Lidar (EarthCARE-ATLID) 355 nm, scheduled for launch in 2020] satellite lidar measurements for their validation and intercomparisons. In addition, ACTIVATE will deploy a new compact multifrequency Profiling Airborne Microwave Radiometer (PAMR) to provide LWP retrievals beyond the redundant measurements by other methods on the HU-25 (from in situ LWC) and B-200 (RSP); these retrievals rely on different physics from that of the RSP and are not significantly affected by assumptions regarding vertical profiles of liquid water (e.g., Zuidema et al. 2012). This combination of remote sensors will enable an additional RSP/PAMR-based retrieval of N_d that is aided by similar subkilometer spatial sampling and has space-based counterparts [e.g., Moderate Resolution Imaging Spectroradiometer (MODIS) and Advanced Microwave Scanning Radiometer 2 (AMSR2)]. Remote sensing retrievals of collocated in situ measurements

MEASUREMENTS-TO-MODELS APPROACH

A hierarchy of modeling tools including large-eddy simulations (LESs), cloud-resolving models (CRMs), a chemical transport model (CTM) and trajectory model, single-column GCM models (SCMs), and full GCMs is employed to study the transport and spatial distribution of aerosol particles, physical and dynamical processes that control the formation and evolution of cloud systems, and the interactions between aerosols and clouds at various spatiotemporal scales (Fig. SB2). The detailed ACTIVATE measurements of meteorological conditions, large-scale forcing, and cloud/aerosol properties, with the innovative sampling strategy, will be used to constrain and evaluate model simulations. CTM and trajectory model simulations will be used to examine transport pathways and quantify source attributions of aerosols. LES/CRM models will be used to gain improved process-level understanding of aerosols, MBL clouds, and their interactions and subsequently to improve the representation of these processes in GCMs. In particular, we will use LES/CRM results to quantify the spectrum of cloud-scale updraft velocity, which is a critical link between clouds and aerosols, and to assess the impact of its crude representation in GCMs on N_a–CCN–N_d relationships. Parameterization evaluations will be first performed in the SCM version of the GCMs. SCM simulations will be constrained with observed or reanalysis [e.g., Modern-Era Retrospective Analysis for Research and Applications, version 2 (MERRA-2)] meteorological and aerosol fields to allow for a better process-level comparison to CRM/LES simulations and observations. Under this framework, the ability of GCMs to simulate the physical/dynamical processes that control the formation/evolution of MBL clouds and interactions with aerosols can be evaluated and improved. The improved parameterizations will then be applied to the corresponding full GCM simulations to directly investigate N_a–CCN–N_d relationships, compared to other GCMs, and evaluated using observations and ACI metrics that can also be provided by current and future satellite missions.

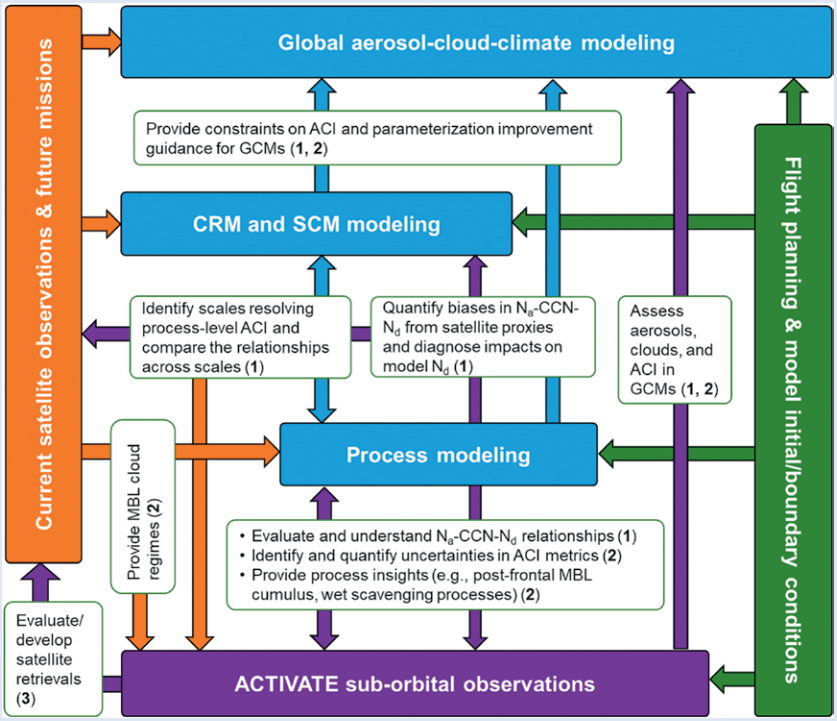

FIG. SB2. Measurements-to-models strategy to address the three science objectives discussed in the "ACTIVATE: A new path forward" section (in bold numbers). Colored boxes denote four ACTIVATE components: preanalysis and flight planning (green), suborbital observations (purple), satellite observations and missions (orange), and modeling hierarchy (blue). Arrows show connections/interactions among the components driven by science objectives (text boxes and bold numbers).

of key ACI microphysical properties (e.g., CCN, N_d, r_e, τ) during ACTIVATE are critical to evaluate and validate advanced retrieval algorithms applicable to both current and future satellite instruments [e.g., MODIS on the NASA *Terra* and *Aqua* satellites, Visible Infrared Imaging Radiometer Suite (VIIRS) on the *Suomi-NPP* and *Joint Polar Satellite System* (*JPSS)-1* satellites, and Advanced Baseline Imager (ABI) on *Geostationary Operational Environmental Satellite* (*GOES)-16* and *-17*].

SUMMARY AND OUTLOOK. Various airborne field campaigns have addressed aerosol–cloud–meteorology interactions during the past two decades. Although these efforts have led to an increase in the sophistication of aerosol and aerosol–cloud interaction treatments in weather and climate models, model uncertainties remain large in part due to a lack of observations purposefully addressing known uncertainties, as well as insufficient measurement statistics. The Decadal Survey (National Academies of Sciences, Engineering, and Medicine 2017) recommends reducing these uncertainties with an approach that ACTIVATE embraces, focused on targeting specific cloud types and integrating multiplatform observations with hierarchical multiscale modeling activities. The overall ACTIVATE strategy is to systematically analyze suborbital observations to advance scientific understanding and evaluate/improve satellite retrievals and global models. Process models with integrated observations bridge the scale and knowledge gaps in between (see sidebar "Measurements-to-models approach").

ACTIVATE also has a comprehensive strategy to reduce parametric and structural uncertainties in the underlying physical parameterization schemes characterizing aerosol–cloud interactions in GCMs. The pragmatic innovation in the sampling strategy with two closely coordinated aircraft is built upon the lessons learned in numerous past field studies including those from the CIRPAS Twin Otter discussed in this work.

ACKNOWLEDGMENTS. ACTIVATE is a NASA Earth Venture Suborbital-3 (EVS-3) investigation, funded by NASA's Earth Science Division and managed through the Earth System Science Pathfinder Program Office. The lead author (A.S.) acknowledges support from NASA grant 80NSSC19K0442 in support of ACTIVATE. The Twin Otter campaigns were sponsored by ONR Grants N00014-11-1-0783, N00014-10-1-0811, N00014-10-1-0200, N00014-04-1-0118, N00014-16-1-2567, N00014-04-1-0018, and N00014-08-1-0465, while E-PEACE was also supported by NSF Grants AGS-1013423 and AGS-1008848. The Pacific Northwest National Laboratory (PNNL) is operated for the U.S. Department of Energy by Battelle Memorial Institute under contract DE-AC05-76RLO1830.

REFERENCES

Alexandrov, M. D., B. Cairns, and M. I. Mishchenko, 2012: Rainbow Fourier transform. *J. Quant. Spectrosc. Radiat. Transfer*, **113**, 2521–2535, https://doi.org/10.1016/j.jqsrt.2012.03.025.

——, and Coauthors, 2018: Retrievals of cloud droplet size from the research scanning polarimeter data: Validation using in situ measurements. *Remote Sens. Environ.*, **210**, 76–95, https://doi.org/10.1016/j.rse.2018.03.005.

Asa-Awuku, A., A. Sorooshian, R. C. Flagan, J. H. Seinfeld, and A. Nenes, 2015: CCN properties of organic aerosol collected below and within marine stratocumulus clouds near Monterey, California. *Atmosphere*, **6**, 1590–1607, https://doi.org/10.3390/atmos6111590.

Bangert, M., C. Kottmeier, B. Vogel, and H. Vogel, 2011: Regional scale effects of the aerosol cloud interaction simulated with an online coupled comprehensive chemistry model. *Atmos. Chem. Phys.*, **11**, 4411–4423, https://doi.org/10.5194/acp-11-4411-2011.

Bauer, S. E., and S. Menon, 2012: Aerosol direct, indirect, semidirect, and surface albedo effects from sector contributions based on the IPCC AR5 emissions for preindustrial and present–day conditions. *J. Geophys. Res.*, **117**, D01206, https://doi.org/10.1029/2011JD016816.

Bennartz, R., 2007: Global assessment of marine boundary layer cloud droplet number concentration from satellite. *J. Geophys. Res.*, **112**, D02201, https://doi.org/10.1029/2006JD007547.

Berg, L. K., and Coauthors, 2016: The Two-Column Aerosol Project: Phase I—Overview and impact of elevated aerosol layers on aerosol optical depth. *J. Geophys. Res. Atmos.*, **121**, 336–361, https://doi.org/10.1002/2015JD023848.

Bodas-Salcedo, A., and Coauthors, 2014: Origins of the solar radiation biases over the Southern Ocean in CFMIP2 models. *J. Climate*, **27**, 41–56, https://doi.org/10.1175/JCLI-D-13-00169.1.

Braun, R. A., and Coauthors, 2018: Cloud adiabaticity and its relationship to marine stratocumulus characteristics over the northeast Pacific Ocean. *J. Geophys. Res. Atmos.*, **123**, 13 790–13 806, https://doi.org/10.1029/2018JD029287.

Castanho, A. D. D., J. V. Martins, P. V. Hobbs, P. Artaxo, L. Remer, M. Yamasoe, and P. R. Colarco, 2005:

Chemical characterization of aerosols on the east coast of the United States using aircraft and ground–based stations during the CLAMS experiment. *J. Atmos. Sci.*, **62**, 934–946, https://doi.org/10.1175/JAS3388.1.

Chen, Y. C., M. W. Christensen, L. Xue, A. Sorooshian, G. L. Stephens, R. M. Rasmussen, and J. H. Seinfeld, 2012: Occurrence of lower cloud albedo in ship tracks. *Atmos. Chem. Phys.*, **12**, 8223–8235, https://doi.org/10.5194/acp-12-8223-2012.

Coggon, M. M., and Coauthors, 2012: Ship impacts on the marine atmosphere: Insights into the contribution of shipping emissions to the properties of marine aerosol and clouds. *Atmos. Chem. Phys.*, **12**, 8439–8458, https://doi.org/10.5194/acp-12-8439-2012.

——, and Coauthors, 2014: Observations of continental biogenic impacts on marine aerosol and clouds off the coast of California. *J. Geophys. Res. Atmos.*, **119**, 6724–6748, https://doi.org/10.1002/2013JD021228.

Crosbie, E., and Coauthors, 2016: Stratocumulus cloud clearings and notable thermodynamic and aerosol contrasts across the clear–cloudy interface. *J. Atmos. Sci.*, **73**, 1083–1099, https://doi.org/10.1175/JAS-D-15-0137.1.

——, and Coauthors, 2018: Development and characterization of a high–efficiency, aircraft–based axial cyclone cloud water collector. *Atmos. Meas. Tech.*, **11**, 5025–5048, https://doi.org/10.5194/amt-11-5025-2018.

Dadashazar, H., and Coauthors, 2017: Relationships between giant sea salt particles and clouds inferred from aircraft physicochemical data. *J. Geophys. Res. Atmos.*, **122**, 3421–3434, https://doi.org/10.1002/2016JD026019.

——, R. A. Braun, E. Crosbie, P. Y. Chuang, R. K. Woods, H. H. Jonsson, and A. Sorooshian, 2018: Aerosol characteristics in the entrainment interface layer in relation to the marine boundary layer and free troposphere. *Atmos. Chem. Phys.*, **18**, 1495–1506, https://doi.org/10.5194/acp-18-1495-2018.

Duong, H. T., A. Sorooshian, and G. Feingold, 2011: Investigating potential biases in observed and modeled metrics of aerosol–cloud–precipitation interactions. *Atmos. Chem. Phys.*, **11**, 4027–4037, https://doi.org/10.5194/acp-11-4027-2011.

Durkee, P. A., and Coauthors, 2000: The impact of ship-produced aerosols on the microstructure and albedo of warm marine stratocumulus clouds: A test of MAST hypotheses 1i and 1ii. *J. Atmos. Sci.*, **57**, 2554–2569, https://doi.org/10.1175/1520-0469(2000)057<2554:TIOSPA>2.0.CO;2.

Ervens, B., A. Sorooshian, Y. B. Lim, and B. J. Turpin, 2014: Key parameters controlling OH-initiated formation of secondary organic aerosol in the aqueous phase (aqSOA). *J. Geophys. Res. Atmos.*, **119**, 3997–4016, https://doi.org/10.1002/2013JD021021.

Fan, J. W., Y. Wang, D. Rosenfeld, and X. H. Liu, 2016: Review of aerosol–cloud interactions: Mechanisms, significance, and challenges. *J. Atmos. Sci.*, **73**, 4221–4252, https://doi.org/10.1175/JAS-D-16-0037.1.

Fast, J. D., and Coauthors, 2016: Model representations of aerosol layers transported from North America over the Atlantic Ocean during the Two-Column Aerosol Project. *J. Geophys. Res. Atmos.*, **121**, 9814–9848, https://doi.org/10.1002/2016JD025248.

Feingold, G., W. R. Cotton, S. M. Kreidenweis, and J. T. Davis, 1999: The impact of giant cloud condensation nuclei on drizzle formation in stratocumulus: Implications for cloud radiative properties. *J. Atmos. Sci.*, **56**, 4100–4117, https://doi.org/10.1175/1520-0469(1999)056<4100:TIOGCC>2.0.CO;2.

——, L. A. Remer, J. Ramaprasad, and Y. J. Kaufman, 2001: Analysis of smoke impact on clouds in Brazilian biomass burning regions: An extension of Twomey's approach. *J. Geophys. Res.*, **106**, 22 907–22 922, https://doi.org/10.1029/2001JD000732.

——, A. McComiskey, D. Rosenfeld, and A. Sorooshian, 2013: On the relationship between cloud contact time and precipitation susceptibility to aerosol. *J. Geophys. Res. Atmos.*, **118**, 10 544–10 554, https://doi.org/10.1002/jgrd.50819.

Field, P. R., R. J. Cotton, K. McBeath, A. P. Lock, S. Webster, and R. P. Allan, 2014: Improving a convection–permitting model simulation of a cold air outbreak. *Quart. J. Roy. Meteor. Soc.*, **140**, 124–138, https://doi.org/10.1002/qj.2116.

——, and Coauthors, 2017: Exploring the convective grey zone with regional simulations of a cold air outbreak. *Quart. J. Roy. Meteor. Soc.*, **143**, 2537–2555, https://doi.org/10.1002/qj.3105.

Gettelman, A., and S. C. Sherwood, 2016: Processes responsible for cloud feedback. *Curr. Clim. Change Rep.*, **2**, 179–189, https://doi.org/10.1007/s40641-016-0052-8.

——, H. Morrison, C. R. Terai, and R. Wood, 2013: Microphysical process rates and global aerosol–cloud interactions. *Atmos. Chem. Phys.*, **13**, 9855–9867, https://doi.org/10.5194/acp-13-9855-2013.

Hair, J., and Coauthors, 2016: Combined atmospheric and ocean profiling from an airborne high spectral resolution lidar. *Epj Web Conf.*, **119**, 22001, https://doi.org/10.1051/epjconf/201611922001.

Hamilton, D. S., L. A. Lee, K. J. Pringle, C. L. Reddington, D. V. Spracklen, and K. S. Carslaw, 2014: Occurrence of pristine aerosol environments on a polluted planet. *Proc. Natl. Acad. Sci. USA*, **111**, 18 466–18 471, https://doi.org/10.1073/pnas.1415440111.

Hartmann, D. L., M. E. Ockertbell, and M. L. Michelsen, 1992: The effect of cloud type on Earth's energy balance: Global analysis. *J. Climate*, **5**, 1281–1304, https://doi.org/10.1175/1520-0442(1992)005<1281:TEOCTO>2.0.CO;2.

Hegg, D. A., D. S. Covert, H. H. Jonsson, and R. K. Woods, 2010: The contribution of anthropogenic aerosols to aerosol light-scattering and CCN activity in the California coastal zone. *Atmos. Chem. Phys.*, **10**, 7341–7351, https://doi.org/10.5194/acp-10-7341-2010.

Hersey, S. P., A. Sorooshian, S. M. Murphy, R. C. Flagan, and J. H. Seinfeld, 2009: Aerosol hygroscopicity in the marine atmosphere: a closure study using high-time-resolution, multiple-RH DASH-SP and size-resolved C-ToF-AMS data. *Atmos. Chem. Phys.*, **9**, 2543–2554, https://doi.org/10.5194/acp-9-2543-2009.

Hostetler, C. A., M. J. Behrenfeld, Y. X. Hu, J. W. Hair, and J. A. Schulien, 2018: Spaceborne lidar in the study of marine systems. *Annu. Rev. Mar. Sci.*, **10**, 121–147, https://doi.org/10.1146/annurev-marine-121916-063335.

IPCC, 2013: *Climate Change 2013: The Physical Science Basis*. Cambridge University Press, 1535 pp., https://doi.org/10.1017/CBO9781107415324.

Jiang, H. L., G. Feingold, and A. Sorooshian, 2010: Effect of aerosol on the susceptibility and efficiency of precipitation in warm trade cumulus clouds. *J. Atmos. Sci.*, **67**, 3525–3540, https://doi.org/10.1175/2010JAS3484.1.

Jung, E., and Coauthors, 2015: Precipitation effects of giant cloud condensation nuclei artificially introduced into stratocumulus clouds. *Atmos. Chem. Phys.*, **15**, 5645–5658, https://doi.org/10.5194/acp-15-5645-2015.

——, B. A. Albrecht, A. Sorooshian, P. Zuidema, and H. H. Jonsson, 2016: Precipitation susceptibility in marine stratocumulus and shallow cumulus from airborne measurements. *Atmos. Chem. Phys.*, **16**, 11 395–11 413, https://doi.org/10.5194/acp-16-11395-2016.

Khairoutdinov, M., and Y. Kogan, 2000: A new cloud physics parameterization in a large–eddy simulation model of marine stratocumulus. *Mon. Wea. Rev.*, **128**, 229–243, https://doi.org/10.1175/1520-0493(2000)128<0229:ANCPPI>2.0.CO;2.

Koren, I., G. Dagan, and O. Altaratz, 2014: From aerosol-limited to invigoration of warm convective clouds. *Science*, **344**, 1143–1146, https://doi.org/10.1126/science.1252595.

Lebo, Z. J., and G. Feingold, 2014: On the relationship between responses in cloud water and precipitation to changes in aerosol. *Atmos. Chem. Phys.*, **14**, 11 817–11 831, https://doi.org/10.5194/acp-14-11817-2014.

Lee, L. A., C. L. Reddington, and K. S. Carslaw, 2016: On the relationship between aerosol model uncertainty and radiative forcing uncertainty. *Proc. Natl. Acad. Sci. USA*, **113**, 5820–5827, https://doi.org/10.1073/pnas.1507050113.

Levy, R. C., S. Mattoo, L. A. Munchak, L. A. Remer, A. M. Sayer, F. Patadia, and N. C. Hsu, 2013: The Collection 6 MODIS aerosol products over land and ocean. *Atmos. Meas. Tech.*, **6**, 2989–3034, https://doi.org/10.5194/amt-6-2989-2013.

Liu, Y. G., and P. H. Daum, 2004: Parameterization of the autoconversion process. Part I: Analytical formulation of the Kessler–type parameterizations. *J. Atmos. Sci.*, **61**, 1539–1548, https://doi.org/10.1175/1520-0469(2004)061<1539:POTAPI>2.0.CO;2.

Lu, M. L., A. Sorooshian, H. H. Jonsson, G. Feingold, R. C. Flagan, and J. H. Seinfeld, 2009: Marine stratocumulus aerosol–cloud relationships in the MASE-II experiment: Precipitation susceptibility in eastern Pacific marine stratocumulus. *J. Geophys. Res.*, **114**, D24203, https://doi.org/10.1029/2009JD012774.

MacDonald, A. B., and Coauthors, 2018: Characteristic vertical profiles of cloud water composition in marine stratocumulus clouds and relationships with precipitation. *J. Geophys. Res. Atmos.*, **123**, 3704–3723, https://doi.org/10.1002/2017JD027900.

Mann, J. A. L., J. C. Chiu, R. J. Hogan, E. J. O'Connor, T. S. L'Ecuyer, T. H. M. Stein, and A. Jefferson, 2014: Aerosol impacts on drizzle properties in warm clouds from ARM Mobile Facility maritime and continental deployments. *J. Geophys. Res. Atmos.*, **119**, 4136–4148, https://doi.org/10.1002/2013JD021339.

Mardi, A. H., and Coauthors, 2018: Biomass burning plumes in the vicinity of the California Coast: Airborne characterization of physicochemical properties, heating rates, and spatiotemporal features. *J. Geophys. Res. Atmos.*, **123**, 13 560–13 582. https://doi.org/10.1029/2018JD029134.

Maudlin, L. C., Z. Wang, H. H. Jonsson, and A. Sorooshian, 2015: Impact of wildfires on size-resolved aerosol composition at a coastal California site. *Atmos. Environ.*, **119**, 59–68, https://doi.org/10.1016/j.atmosenv.2015.08.039.

McComiskey, A., and G. Feingold, 2012: The scale problem in quantifying aerosol indirect effects. *Atmos. Chem. Phys.*, **12**, 1031–1049, https://doi.org/10.5194/acp-12-1031-2012.

McComiskey, A., G. Feingold, A. S. Frisch, D. D. Turner, M. A. Miller, J. C. Chiu, Q. Min, and J. A. Ogren, 2009: An assessment of aerosol-cloud interactions in marine stratus clouds based on surface remote sensing. *J. Geophys. Res.*, 114, D09203, https://doi.org/10.1029/2008JD011006.

McCoy, D. T., and Coauthors, 2015: Natural aerosols explain seasonal and spatial patterns of Southern Ocean cloud albedo. *Sci. Adv.*, 1, e1500157, https://doi.org/10.1126/sciadv.1500157.

Mechoso, C., and Coauthors, 2014: Ocean–Cloud–Atmosphere–Land Interactions in the Southeast Pacific: The VOCALS Program. *Bull. Amer. Meteor. Soc.*, **95**, 357–375, https://doi.org/10.1175/BAMS-D-11-00246.1.

Merikanto, J., D. V. Spracklen, K. J. Pringle, and K. S. Carslaw, 2010: Effects of boundary layer particle formation on cloud droplet number and changes in cloud albedo from 1850 to 2000. *Atmos. Chem. Phys.*, **10**, 695–705, https://doi.org/10.5194/acp-10-695-2010.

Minnis, P., and Coauthors, 2011: CERES Edition-2 cloud property retrievals using TRMM VIRS and Terra and Aqua MODIS data—Part I: Algorithms. *IEEE Ttrans. Geosci. Remote Sens.*, **49**, 4374–4400, https://doi.org/10.1109/TGRS.2011.2144601.

Modini, R. L., and Coauthors, 2015: Primary marine aerosol–cloud interactions off the coast of California. *J. Geophys. Res. Atmos.*, **120**, 4282–4303, https://doi.org/10.1002/2014JD022963.

Müller, D., and Coauthors, 2014: Airborne Multiwavelength High Spectral Resolution Lidar (HSRL-2) observations during TCAP 2012: Vertical profiles of optical and microphysical properties of a smoke/urban haze plume over the northeastern coast of the US. *Atmos. Meas. Tech.*, **7**, 3487–3496, https://doi.org/10.5194/amt-7-3487-2014.

Mülmenstädt, J., and G. Feingold, 2018: *Curr. Climate Change Rep.*, **4**, 23, https://doi.org/10.1007/s40641-018-0089-y.

National Academies of Sciences, Engineering, and Medicine, 2017: The 2017–2027 Decadal Survey for Earth Science and Applications from Space (ESAS 2017). National Academy of Sciences, http://sites.nationalacademies.org/DEPS/ESAS2017/index.htm.

Painemal, D., 2018: Global estimates of changes in shortwave low-cloud albedo and fluxes due to variations in cloud droplet number concentration derived from CERES-MODIS satellite sensors. *Geophys. Res. Lett.*, **45**, 9288–9296, https://doi.org/10.1029/2018GL078880.

——, and P. Zuidema, 2013: The first aerosol indirect effect quantified through airborne remote sensing during VOCALS–REx. *Atmos. Chem. Phys.*, **13**, 917–931, https://doi.org/10.5194/acp-13-917-2013.

Prabhakar, G., B. Ervens, Z. Wang, L. C. Maudlin, M. M. Coggon, H. H. Jonsson, J. H. Seinfeld, and A. Sorooshian, 2014: Sources of nitrate in stratocumulus cloud water: Airborne measurements during the 2011 E-PEACE and 2013 NiCE studies. *Atmos. Environ.*, **97**, 166–173, https://doi.org/10.1016/j.atmosenv.2014.08.019.

Randles, C. A., and Coauthors, 2017: The MERRA-2 aerosol reanalysis, 1980 onward. Part I: System description and data assimilation evaluation. *J. Climate*, **30**, 6823–6850, https://doi.org/10.1175/JCLI-D-16-0609.1.

Remillard, J., and G. Tselioudis, 2015: Cloud regime variability over the Azores and its application to climate model evaluation. *J. Climate*, **28**, 9707–9720, https://doi.org/10.1175/JCLI-D-15-0066.1.

Russell, L. M., and Coauthors, 2013: Eastern Pacific Emitted Aerosol Cloud Experiment. *Bull. Amer. Meteor. Soc.*, **94**, 709–729, https://doi.org/10.1175/BAMS-D-12-00015.1.

Sanchez, K. J., and Coauthors, 2016: Meteorological and aerosol effects on marine cloud microphysical properties. *J. Geophys. Res. Atmos.*, **121**, 4142–4161, https://doi.org/10.1002/2015JD024595.

Sawamura, P., and Coauthors, 2017: HSRL-2 aerosol optical measurements and microphysical retrievals vs. airborne in situ measurements during DISCOVER-AQ 2013: An intercomparison study. *Atmos. Chem. Phys.*, **17**, 7229–7243, https://doi.org/10.5194/acp-17-7229-2017.

Schulien, J. A., M. J. Behrenfeld, J. W. Hair, C. A. Hostetler, and M. S. Twardowski, 2017: Vertically-resolved phytoplankton carbon and net primary production from a high spectral resolution lidar. *Opt. Express*, **25**, 13 577–13 587, https://doi.org/10.1364/OE.25.013577.

Seinfeld, J. H., and Coauthors, 2016: Improving our fundamental understanding of the role of aerosol–cloud interactions in the climate system. *Proc. Natl. Acad. Sci. USA*, **113**, 5781–5790, https://doi.org/10.1073/pnas.1514043113.

Shingler, T., and Coauthors, 2012: Characterisation and airborne deployment of a new counterflow virtual impactor inlet. *Atmos. Meas. Tech.*, **5**, 1259–1269, https://doi.org/10.5194/amt-5-1259-2012.

——, and Coauthors, 2016: Ambient observations of hygroscopic growth factor and f(RH) below 1: Case studies from surface and airborne measurements. *J. Geophys. Res. Atmos.*, **121**, 13 661–13 677, https://doi.org/10.1002/2016JD025471.

Sorooshian, A., M. L. Lu, F. J. Brechtel, H. Jonsson, G. Feingold, R. C. Flagan, and J. H. Seinfeld, 2007: On the source of organic acid aerosol layers above clouds. *Environ. Sci. Technol.*, **41**, 4647–4654, https://doi.org/10.1021/es0630442.

——, and Coauthors, 2009a: On the link between ocean biota emissions, aerosol, and maritime clouds:

Airborne, ground, and satellite measurements off the coast of California. *Global Biogeochem. Cycles*, **23**, GB4007, https://doi.org/10.1029/2009GB003464.

——, G. Feingold, M. D. Lebsock, H. L. Jiang, and G. L. Stephens, 2009b: On the precipitation susceptibility of clouds to aerosol perturbations. *Geophys. Res. Lett.*, **36**, L13803, https://doi.org/10.1029/2009GL038993.

——, S. M. Murphy, S. Hersey, R. Bahreini, H. Jonsson, R. C. Flagan, and J. H. Seinfeld, 2010a: Constraining the contribution of organic acids and AMS *m/z* 44 to the organic aerosol budget: On the importance of meteorology, aerosol hygroscopicity, and region. *Geophys. Res. Lett.*, **37**, L21807, https://doi.org/10.1029/2010GL044951.

——, G. Feingold, M. D. Lebsock, H. L. Jiang, and G. L. Stephens, 2010b: Deconstructing the precipitation susceptibility construct: Improving methodology for aerosol–cloud precipitation studies. *J. Geophys. Res.*, **115**, D17201, https://doi.org/10.1029/2009JD013426.

——, Z. Wang, M. M. Coggon, H. H. Jonsson, and B. Ervens, 2013: Observations of sharp oxalate reductions in stratocumulus clouds at variable altitudes: Organic acid and metal measurements during the 2011 E-PEACE Campaign. *Environ. Sci. Technol.*, **47**, 7747–7756, https://doi.org/10.1021/es4012383.

——, G. Prabhakar, H. Jonsson, R. K. Woods, R. C. Flagan, and J. H. Seinfeld, 2015a: On the presence of giant particles downwind of ships in the marine boundary layer. *Geophys. Res. Lett.*, **42**, 2024–2030, https://doi.org/10.1002/2015GL063179.

——, and Coauthors, 2015b: Surface and airborne measurements of organosulfur and methanesulfonate over the western United States and coastal areas. *J. Geophys. Res. Atmos.*, **120**, 8535–8548, https://doi.org/10.1002/2015JD023822.

——, and Coauthors, 2017: A multi–year data set on aerosol-cloud-precipitation-meteorology interactions for marine stratocumulus clouds. Figshare, https://doi.org/10.6084/m9.figshare.5099983.v3.

——, and Coauthors, 2018: A multi-year data set on aerosol-cloud-precipitation-meteorology interactions for marine stratocumulus clouds. *Sci. Data*, **5**, 180026, https://doi.org/10.1038/sdata.2018.26.

Stamnes, S., and Coauthors, 2018: Simultaneous polarimeter retrievals of microphysical aerosol and ocean color parameters from the "MAPP" algorithm with comparison to high-spectral-resolution lidar aerosol and ocean products. *Appl. Opt.*, **57**, 2394–2413, https://doi.org/10.1364/AO.57.002394.

Stevens, B., and G. Feingold, 2009: Untangling aerosol effects on clouds and precipitation in a buffered system. *Nature*, **461**, 607–613, https://doi.org/10.1038/nature08281.

Terai, C. R., R. Wood, D. C. Leon, and P. Zuidema, 2012: Does precipitation susceptibility vary with increasing cloud thickness in marine stratocumulus? *Atmos. Chem. Phys.*, **12**, 4567–4583, https://doi.org/10.5194/acp-12-4567-2012.

Terai, C. R., R. Wood, and T. L. Kubar, 2015: Satellite estimates of precipitation susceptibility in low-level marine stratiform clouds. *J. Geophys. Res. Atmos.*, **120**, 8878–8889, https://doi.org/10.1002/2015JD023319.

Trenberth, K. E., and J. T. Fasullo, 2010: Simulation of present-day and twenty-first-century energy budgets of the Southern Oceans. *J. Climate*, **23**, 440–454, https://doi.org/10.1175/2009JCLI3152.1.

Tselioudis, G., W. Rossow, Y. C. Zhang, and D. Konsta, 2013: Global weather states and their properties from passive and active satellite cloud retrievals. *J. Climate*, **26**, 7734–7746, https://doi.org/10.1175/JCLI-D-13-00024.1.

Wang, Z., A. Sorooshian, G. Prabhakar, M. M. Coggon, and H. H. Jonsson, 2014: Impact of emissions from shipping, land, and the ocean on stratocumulus cloud water elemental composition during the 2011 E-PEACE field campaign. *Atmos. Environ.*, **89**, 570–580, https://doi.org/10.1016/j.atmosenv.2014.01.020.

——, and Coauthors, 2016: Contrasting cloud composition between coupled and decoupled marine boundary layer clouds. *J. Geophys. Res. Atmos.*, **121**, 11 679–11 691, https://doi.org/10.1002/2016JD025695.

Warren, S. G., C. J. Hahn, J. London, R. M. Chervin, and R. L. Jenne, 1998: Global distribution of total cloud cover and cloud types over ocean. NCAR Tech. Note NCAR/TN-317+STR, 42 pp., https://doi.org/10.5065/D6QC01D1.

Weiss-Penzias, P., and Coauthors, 2018: Aircraft measurements of total mercury and monomethyl mercury in summertime marine stratus cloudwater from coastal California, USA. *Environ. Sci. Technol.*, **52**, 2527–2537, https://doi.org/10.1021/acs.est.7b05395.

Williams, K. D., and Coauthors, 2013: The Transpose-AMIP II experiment and its application to the understanding of Southern Ocean cloud biases in climate models. *J. Climate*, **26**, 3258–3274, https://doi.org/10.1175/JCLI-D-12-00429.1.

Wonaschütz, A., and Coauthors, 2013: Hygroscopic properties of smoke-generated organic aerosol particles emitted in the marine atmosphere. *Atmos. Chem. Phys.*, **13**, 9819–9835, https://doi.org/10.5194/acp-13-9819-2013.

Wood, R., 2005: Drizzle in stratiform boundary layer clouds. Part II: Microphysical aspects. *J. Atmos. Sci.*, **62**, 3034–3050, https://doi.org/10.1175/JAS3530.1.

——, T. L. Kubar, and D. L. Hartmann, 2009: Understanding the importance of microphysics and macrophysics for warm rain in marine low clouds. Part II: Heuristic models of rain formation. *J. Atmos. Sci.*, **66**, 2973–2990, https://doi.org/10.1175/2009JAS3072.1.

——, and Coauthors, 2016: Planning the next decade of coordinated research to better understand and simulate marine low clouds. *Bull. Amer. Meteor. Soc.*, **97**, 1699–1702, https://doi.org/10.1175/BAMS-D-16-0160.1.

——, J. D. Stemmler, J. Remillard, and A. Jefferson, 2017: Low-CCN concentration air masses over the eastern North Atlantic: Seasonality, meteorology, and drivers. *J. Geophys. Res. Atmos.*, **122**, 1203–1223, https://doi.org/10.1002/2016JD025557.

Xu, F., and Coauthors, 2018: Coupled retrieval of liquid water cloud and above-cloud aerosol properties using the Airborne Multiangle SpectroPolarimetric Imager (AirMSPI). *J. Geophys. Res. Atmos.*, **123**, 3175–3204, https://doi.org/10.1002/2017JD027926.

Yoon, J., J. P. Burrows, M. Vountas, W. von Hoyningen-Huene, D. Y. Chang, A. Richter, and A. Hilboll, 2014: Changes in atmospheric aerosol loading retrieved from space-based measurements during the past decade. *Atmos. Chem. Phys.*, **14**, 6881–6902, https://doi.org/10.5194/acp-14-6881-2014.

Youn, J. S., E. Crosbie, L. C. Maudlin, Z. Wang, and A. Sorooshian, 2015: Dimethylamine as a major alkyl amine species in particles and cloud water: Observations in semi-arid and coastal regions. *Atmos. Environ.*, **122**, 250–258, https://doi.org/10.1016/j.atmosenv.2015.09.061.

Zuidema, P., D. Painemal, S. de Szoeke, and C. Fairall, 2009: Stratocumulus cloud-top height estimates and their climatic implications. *J. Climate*, **22**, 4652–4666, https://doi.org/10.1175/2009JCLI2708.1.

——, D. Leon, A. Pazmany, and M. Cadeddu, 2012: Aircraft millimeter-wave passive sensing of cloud liquid water and water vapor during VOCALS-REx. *Atmos. Chem. Phys.*, **12**, 355–369, https://doi.org/10.5194/acp-12-355-2012.